Talanta 118 (2014) 45–53

Contents lists available at ScienceDirect

Talanta

journal homepage: www.elsevier.com/locate/talanta

# Ultrahigh resolution mass spectrometry-based metabolic characterization reveals cerebellum as a disturbed region in two animal models

Shuhai Lin [a,1], Basem Kanawati [b,1], Liangfeng Liu [c], Michael Witting [b], Min Li [c], Jiandong Huang [d], Philippe Schmitt-Kopplin [b,e,*], Zongwei Cai [a,**]

[a] Department of Chemistry, Hong Kong Baptist University, Hong Kong SAR, China
[b] Analytical Biogeochemistry, Helmholtz-Zentrum Muenchen-German Research Center for Environmental Health, Ingolstaedter Landstrasse 1, D-85764 Oberschleißheim, Germany
[c] School of Chinese Medicine, Hong Kong Baptist University, Hong Kong SAR, China
[d] Department of Biochemistry, The University of Hong Kong, Hong Kong SAR, China
[e] Analytical Food Chemistry, Technische Universität München, D-85354 Freising-Weihenstephan, Germany

ARTICLE INFO

*Article history:*
Received 18 June 2013
Received in revised form
7 September 2013
Accepted 16 September 2013
Available online 5 October 2013

*Keywords:*
FT-ICR/MS
Tg CRND8 mice
TCDD exposure
Chemical profiles
Cerebellum

ABSTRACT

In the previous reports about cognitive dysfunction, cerebellum was thought to be a less affected tissue by genetic or environmental alterations in comparison to other tissues in the brain including hippocampus under the same conditions. In this work, we investigated two types of metabolomic alterations inside the cerebellum tissue. The first one addressed the differences in the metabolomics profiles between Transgenic (Tg) CRND8 of Alzheimer's disease mice and non-transgenic (non-Tg) littermates. The second one addressed the metabolic differences between wild type mice exposed to 2,3,7,8-tetrachlorodibenzo-*p*-dioxin (TCDD) and wild type mice which are not exposed to this toxic compound. For these two investigations, ultrahigh resolution Fourier transform ion cyclotron resonance mass spectrometry (FT-ICR/MS) was implemented. As a result, the significant changes of each comparison were tentatively annotated by the high mass accuracy generated from the measurements in the negative ion mode. The biosynthesis of amino acids was also enhanced pronouncedly, and perturbation of purine metabolism was also observed in Tg mice compared to non-Tg littermates. In another animal model, the reduced levels of amino acids were found whereas the intermediate levels in purine metabolism and fatty acids including fatty acid conjugated metabolites were elevated in cerebellar tissues of mice exposed to TCDD compared to control group. Collectively, it was demonstrated that FT-ICR/MS was a powerful tool for interpretation of the elemental compositions of the peaks, revealing that the metabolic perturbations in cerebellar tissues of mice were induced by either genetic manipulation or environmental factor. Therefore, the non-targeted approach, alternatively, provides various metabolic phenotypes for the systems-level mirror of the complex etiology of neurotoxicity in the cerebellum.



## 1. Introduction

Alzheimer's disease (AD) is a progressive neurodegenerative disease and characterized by memory deficits, cognitive decline and ultimately complete loss of intellectual ability [1]. A variety of murine models are generated primarily by the overexpression of wild-type amyloid precursor protein (APP) or APP with mutations [2]. Selective neuronal degeneration in the brain of AD has been observed to understand the resistance of cerebellum to toxic effect [3]. More interestingly, the metabolites of cerebellar neurons were found to significantly reduce brain A$\beta$ levels and reverse cognitive impairments and other AD-like phenotypes of APP/PS1 transgenic mice, in both early and late stages of AD pathology, although the metabolites of cerebellar neurons were not identified; whereas the metabolites of hippocampal neurons play the opposite role in pathogenesis of AD [4]. The growing evidence shows that cerebellum in AD brain could partially protect itself from A$\beta$ or Tau-induced toxicity.

In this regard, we attempted to investigate the cerebellum from different types of mouse models using a novel tool. First of all, transgenic (Tg) CRND8 mouse model was chosen to be the experimental animal. The expression of both the Swedish mutation and the V717F mutation in Tg CRND8 mice cause early

* Corresponding author at: Analytical Biogeochemistry, Helmholtz-Zentrum Muenchen-German Research Center for Environmental Health, Ingolstaedter Landstrasse 1, D-85764 Oberschleißheim, Germany.
** Corresponding author. Tel.: +852 34117070; fax: +852 34117348.
*E-mail addresses:* schmitt-kopplin@helmholtz-muenchen.de (P. Schmitt-Kopplin), zwcai@hkbu.edu.hk (Z. Cai).
[1] These authors contributed equally to this work.

0039-9140/$ - see front matter © 2013 Elsevier B.V. All rights reserved.
http://dx.doi.org/10.1016/j.talanta.2013.09.019

deposition of amyloid in plaques and premature death dependent, indicating the importance of genetic background on the effects of APP overexpression [5,6]. Furthermore, we used the extremely toxic compound, 2,3,7,8-tetrachlorodibenzo-*p*-dioxin (TCDD), to treat the wild-type mice. The notorious environmental toxicant, possesses a broad spectrum of the adverse effects on human health. Recent evidence has demonstrated that dioxin disturbs various aspects of sexuality, including subtle endocrine, developmental, neurological, and immunological effects, in addition being a potent carcinogen [7]. We previously conducted animal models to examine the metabolic traits in biofluid, liver and skeletal muscle tissues of mice exposed to TCDD, and also found that TCDD could accelerate ageing in rats [8–10]. Therefore, the cerebellar tissues were collected from these animals for metabolomic analysis.

Metabolomics provides such an approach to record the phenotypic changes. To address the metabolic signatures in cerebellum of mice, ultrahigh resolution mass spectrometry was employed to track the metabolites. Fourier transform ion cyclotron resonance mass spectrometry (FT-ICR/MS) provides very fine isotopic distribution as well as high mass accuracy for metabolite identification. When combining electrospray ionization (ESI), FT-ICR detection could yield striking results in the analysis of the formed ions. It should be mentioned that the mass resolving power significantly increases with lower $m/z$ ratios. This means that the implementation of FT-ICR/MS in metabolomic studies is of great advantage, since most of the metabolites have $m/z$ ratios lower than 700. Moreover, FT-ICR/MS allows direct infusion analyses of crude biological samples without previous chromatographic separation steps and derivatization reactions, and high-throughput metabolic profiling studies were done for functional characterization of novel genes [11]. For instance, the non-targeted metabolic profiling based on FT-ICR/MS discriminated six different varieties of maize [12]. Furthermore, the elemental compositions of analytes can be estimated with the aid of accurate mass measurement leading to the prediction of possible metabolite candidates [13]. To date, FT-ICR/MS has been used for metabolome investigations, such as Crohn's disease [14], insulin sensitivity [15]. Additionally, an unprecedented chemical diversity of wine composition was uncovered for the metabologeographic signature of the forest location for wine elaboration [16].

Therefore, this work intended to investigate the chemical profiles in cerebellum of either Tg CRND8 mice versus non-Tg littermates or the wild-type mice which were exposed to TCDD in comparison to those in control group. In these two studies, chemical profiles in cerebellum of mice would witness a diversity of small molecules affected by genetic modification or environmental influence using ultrahigh resolution FT-ICR/MS.

## 2. Material and methods

### 2.1. Animal experiments

Male Tg CRND8 mice and non-Tg littermates were provided by Li Ka Shing Faculty of Medicine, the University of Hong Kong and acclimatized in our animal laboratory. Male C57BL/6J wild-type mice were purchased from Chinese University of Hong Kong, Hong Kong SAR, China. All animal experiments were conducted according to the guidelines established by the NIH Guide for the Care and Use of Laboratory Animals. Two categories of animal models were used in this work: Tg CRND8 mice of Alzheimer's disease versus non-Tg littermates; C57BL/6J wild-type mice exposed to TCDD versus control group ($n=6$ for each group). 20-week male Tg CRND8 and age-matched male non-Tg littermates were decapitated for dissecting the cerebellum tissues. For transgenic discrimination, animals were confirmed and separated by polymerase chain reaction for assaying the brain tissues. Four-weeks male wild-type mice were treated with a single administration of either single dose (10 μg $kg^{-1}$ TCDD dissolved in corn oil) or 5 mL $kg^{-1}$ corn oil as the control group. The mice which were exposed to TCDD as well as control group were sacrificed at 12th week after the administration to harvest the cerebellum tissues. The tissues were stored at −80 °C prior to sample preparation.

### 2.2. Sample preparation

An amount of 20 mg of each tissue was stored at −20 °C. Protein precipitation was performed by adding 1 mL solvent mixture (methanol/water 4:1, $v/v$) to 2 mL eppendorf tubes. Samples were vortexed for 30 s and submerged 2–3 min in liquid nitrogen and then thawed for three minutes and sonicated for two minutes. This process was repeated three times and samples were stored at −20 °C for 1 h. The supernatant was removed by centrifugation at 12,000 rpm for ten minutes. The supernatant was transferred to a clean tube and dried in SpeedVac. The residue was re-dissolved in 500 μL of cold acetonitrile/water (50:50, $v/v$) containing 0.1% formic acid. The supernatant was collected after centrifugation at 12,000 rpm for ten minutes and the solution was stored at −20 °C prior to analysis. The solution was diluted 100 times using 70% methanol for FT-ICR/MS measurement. The use of 70% methanolic solution for mass spectrometric analysis was helpful to get highest ionization efficiency. A 30% water partition was kept in the injected solutions in order to ensure that all metabolites are accommodated in solution so that no precipitation of important metabolites, which do not dissolve in pure methanol can occur.

### 2.3. Mass spectrometric conditions

High-resolution mass spectra for molecular formula assignments were acquired on a Fourier Transform Ion Cyclotron Resonance Mass Spectrometry (FT-ICR/MS, Solarix, Bruker Daltonics, Bremen, Germany) equipped with a 12-T superconducting magnet and an Apollo II electrospray ion (ESI) source. Each sample was introduced into the ionization source at a flow rate of 2 μL $min^{-1}$ by a microliter pump with a nebulizer gas pressure of 20 psi and a drying gas pressure of 15 psi (heated to 200 °C). All samples were measured three times in negative ionization electrospray mode. The samples were also detected in positive ion mode. However, the results from negative ion mode showed more significant biomarkers for metabolic implications.

The instrument was calibrated based on cluster ions of 5 mg $L^{-1}$ arginine in methanol. Calibration errors in the relevant mass range were always below 0.05 ppm. The spectra were acquired with a time domain transient length of two Mega words with mass range between 123 and 1000 $m/z$. Each transient gave a mass resolving power of more than 190,000 at $m/z=400$. Three hundred scans with duration of 15 min were summed up in each acquisition. The ion accumulation time in the ion source was set to 100 ms.

### 2.4. Data analysis

FT-ICR mass spectra were exported to peak lists at a signal to noise ratio ($S/N$) of 3. A mass scale unification was performed by using the home made software: matrix generator, and the window width was set at 1 ppm for this purpose. 80% rule was applied for data preprocessing. The 80% rule was conducted for all variables (masses) in the data set in order to remove all variables (masses) which possess number of zero intensity values that exceed 20% of each sample class [17]. This data filtration was performed in MATLAB 2009b (MathWorks, Inc. USA).

Principal components analysis (PCA) was also performed in SIMCA-P 12.0.1 (Umetrics, Sweden). In addition, the differential ions were implemented into MassTRIX interface (http://www.masstrix.org)

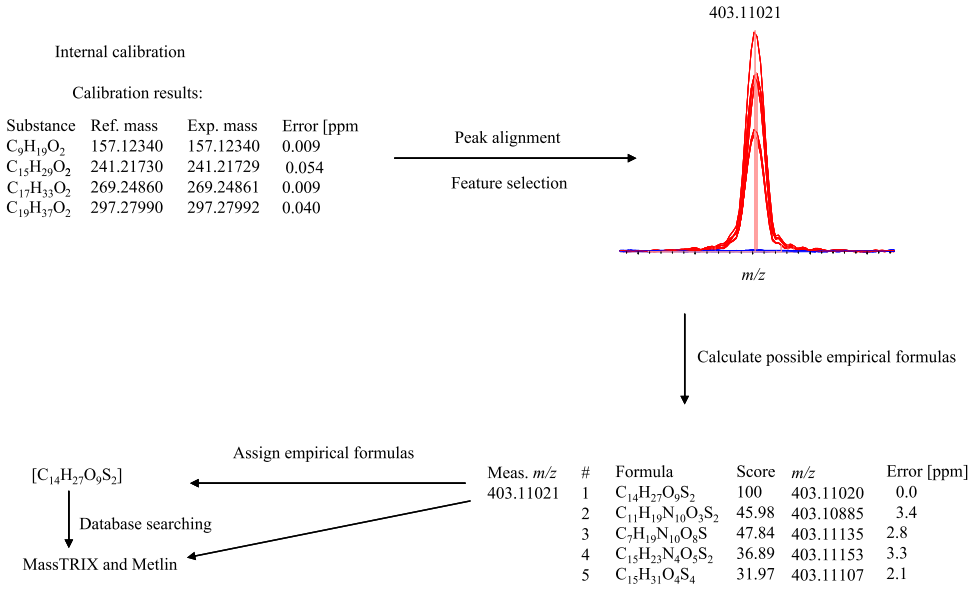


**Scheme 1.** The procedure of assigning an empirical formula to mass peaks. The internal calibration was performed by using the ESI library of fatty acids in the negative ion mode. Linear calibration was adopted. Mass error $<0.1$ ppm was obtained in the calibration. Peaks (from different mass spectra) which belong to the same mass were aligned by performing a linear calibration and mass lists were produced. After peak alignment, the differential ions were selected by performing profile search in HCE software for calculating the empirical formulas in DataAnalysis program (Bruker, Bremen, Germany). Meanwhile, the accuracy mass was accessible with the massTRIX interface or Metlin database. Moreover, the putative biomarkers were simulated into the metabolic pathways.

and Metlin (http://metlin.scripps.edu/) to search for the identified discriminant masses [18]. The criteria in the database search were as follows: negative ionization (correct for $H^+$ loss) was selected as the scan mode; maximum error was set to 1.0 ppm. KEGG with expanded lipids (HMDB, LipidMaps) (2006–2009) and Mus Musculus (mouse) were chosen for the database and organism, respectively. Cluster heat map was generated using hierarchical clustering explorer (http://www.cs.umd.edu/hcil/hce/). Because metabolic pathways were proposed for a better understanding, a web-tool MetaboAnalyst 2.0 (http://www.metaboanalyst.ca/) was used for the pathway analysis and visualization.

Scheme 1 shows the necessary steps that were taken in order to perform the complete data analysis: mass calibration followed by peak alignment, mass scale unification and statistical multivariative data analysis. This produces discriminant masses which were subsequently validated in the stacked view. The validated discriminant masses were assigned to specific sum formulae and the highly accurate masses were uploaded to MassTRIX and Metlin for database search (Scheme 1). Not all found discriminant masses could be annotated as a result of the database search but those annotated metabolites are discussed below in more details.

## 3. Results and discussion

### 3.1. Description of the chemical spaces

Cognitive dysfunction was testified in Tg CRND8 mice by investigating cerebral cortex [19]. However, the metabolic changes in cerebellum as the pathogenesis of Alzheimer's disease remain elusive. Owing to the high mass resolving power and high mass accuracy of the FT-ICR/MS, a holistic non-targeted approach enables producing an instant molecular picture of cerebellum. As a result of the data filtration procedure mentioned above (80% rule), the data set of cerebellum in AD model (Tg versus non-Tg) measured in negative ion mode was reduced from 136,497 features to 3171 features while the data of cerebellum in TCDD model (dosage group versus control group) measured in negative ion mode was reduced from 161,478 features to 5292 features.

When these extracts were subjected to a high magnetic field (12 T) FT-ICR/MS, several thousands to more than ten thousands of highly resolved mass signals were observed within a mass range of *m/z* 123–1000 *m/z* (Fig. 1A) and the zoom in mass spectrum within a mass range of *m/z* 250–350 Da (Fig. 1B). Error margins routinely as low as $<100$ ppb in internal calibration cleared the way to assign individual mass peaks to their corresponding unique elemental compositions within these error levels. The spectrum acquired in the ESI($-$) mode delivered ionic elemental formulae at the *m/z* 297 nominal mass ion with up to five elemental compositions assigned with only 0.26 Da *m/z* window (Fig. 1C). As shown in the Venn diagram in Fig. 1D, most features are observed in both Tg and non-Tg samples, but a significant number are unique to a given sample set, with $\sim$3-fold more ions in the Tg samples unique to the non-Tg samples in negative ion mode, indicating that Tg group has more detected ions. Similarly, the unique ions in control group of TCDD model are two times of those in dosage group, indicating that TCDD exposure causes less detected ions in the samples. Furthermore, we performed principal components analysis (PCA) of the profiling data analyzed in negative ion mode from home-made Matrix Generator filtered by 80% rule and this shows a clear separation between sample groups: Tg and non-Tg (Fig. 1E).

Due to the high mass accuracy, normally each mass could yield a unique molecular formula within a mass tolerance of 1.0 ppm with $^{13}C$-isotope. But notably, the molecular formulas should be validated by the rules mentioned below. Previously, Kind and Fiehn reported that seven golden rules for heuristic filtering of the molecular formulas exist [20]. Here, we introduced a new rule by using partial least square-discriminant analysis (PLS-DA). It is well-known that supervised method PLS-DA could be used for feature selection. PLS-DA was conducted for the classification of the different groups in Fig. 1S for AD model (See Supporting information). The parameters in the score plot are important to evaluate the robustness of a pattern recognition model. *R2*(*Y*) is 99.7% and *Q2* is 91.8%, indicating the clear classification in this model. Typically, the differentiating mass which embraces variable importance of project (VIP) $>1.0$ could be considered to be an important feature. Similarly, the feature selection was conducted for other data sets. In another TCDD model, unsupervised PCA and supervised PLS-DA models were performed in the

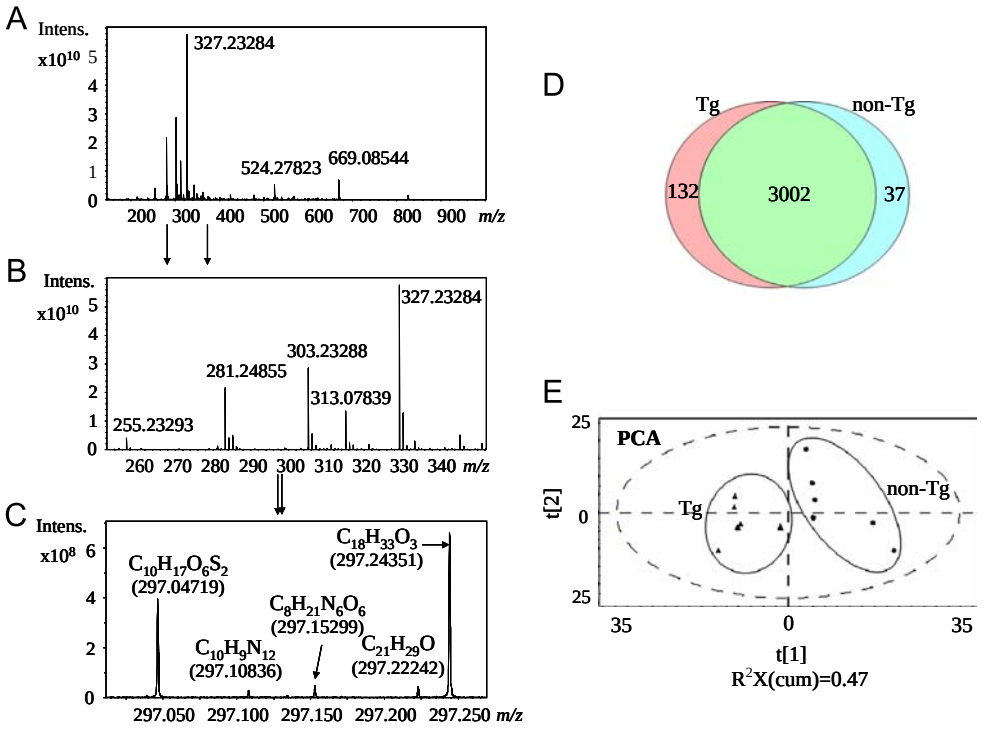


**Fig. 1.** The visualization of the methanolic cerebellum extract in the ESI(−) FT-ICR/MS spectra in the mass ranges (A) 123–1000 Da, (B) 250–350 Da, and (C) 297.00–297.26 Da with credible elemental formula assignments. (D) As shown in the Venn diagram, most features are observed in both Tg and non-Tg samples, but a significant number are unique to a given sample set, with ~3-fold more ions in the Tg samples unique to the non-Tg samples in negative ion mode. (E) Principal components analysis of the profiling data analyzed in negative ion mode from Matrix Generator filtered by 80% rule shows the separation between sample groups: Tg and non-Tg (R2X(cum)=0.47).

grouping (Fig. 2SA and B). Not surprisingly, PLS-DA model displays the good cross-validation evaluated by the parameters $R2(Y)=99\%$ and $Q2=81.9\%$. In the 5292 masses, up to 2433 variables (masses) have the VIP > 1.0. However, the variables which have negative Q2 values should be deleted from the table for the tested groups. Moreover, through *t*-test recalculation, the masses with *P*-value < 0.05 were considered to be significant changes. Subsequently, metabolite identification was carried out in MassTRIX interface. However, some of the differential masses could not be annotated in the biological databases. In this regard, we calculated the sum formulae of the true discriminant masses and validated these sum formulas by istotope pattern matching using the FT-ICR/MS software DataAnalysis, and then the molecular formulas would be validated by ChemSpider database (http://www.chemspider.com/). If the molecular formulas could not be hit in ChemSpider database, they will be considered as invalid elemental compositions [21]. We would also like to take one more example to explain this procedure in Fig. S3. In the very fine mass spectra, the difference between Tg and non-Tg samples could be reflected by the sensitive measurement with ultrahigh resolution (Fig. S3A and B). The unique ion at *m*/*z* 285.06525 in Tg samples was assigned to be propyl 6-deoxy-6-sulfohexopyranoside by searching against ChemSpider database. Meanwhile, another unique ion at *m*/*z* 298.05061 corresponding to $C_{11}H_{13}N_3O_5S$ has up to 106 hits in ChemSpider database. Similarly, the ion at *m*/*z* 313.07839 was assigned to $[C_{11}H_{21}O_6S_2]^-$. The isotopic distribution was figured out (Fig. S4). Surprisingly, the metabolite was enhanced markedly (up to 241.97-fold) in Tg cerebellum compared to non-Tg cerebellum (Fig. S4D). In contrast, this sulfur-containing metabolite was also observed in the reduced level of cerebellar tissue of TCDD exposure group.

### 3.2. Imbalance of sulfur-containing metabolites

By means of *P*-values, we selected the mass profiles which significantly changed in two groups in AD model. Simulated by DataAnalysis program, a total of 12 sulfur-containing formulas were highlighted in Table S1. Furthermore, these formulas were also calculated in TCDD model (TCDD exposure versus control group). All of the formulas were evaluated by the following rules. Firstly, double bond equivalents (DBEs) were calculated from elemental compositions using the following equation, on the basis of the elemental formula $CcHhNnOoSsPp$:

$DBE=c-h/2+n/2+p/2+1$. The number of valence electrons considered for phosphorus is 3 [22].

Secondly, the upper limit for the DBE to carbon is 90% of the carbon number and the DBE lower limit is zero, which is termed "90% rule" [23]. Thirdly, other two rules are that the number of *n* over *c* should be equal or less than 1, and $(o+n)/c$ should be less than 3 to make sure that the assigned sum formulae have chemical meaning.

It is worth to note that several unique sulfur-containing metabolites were highlighted in Table S1 are induced by genetic or environmental alteration. These distinct mass profiles imply the strong patterns of relationships for understanding the role of sulfur-containing metabolites in cerebellar tissues of mice. Indeed, sulfur-containing substances in rat livers have been annotated by metabolomic analysis [24]. However, due to database limitation which cannot follow up the broad band detected variety of signals obtained from ultrahigh resolution of FT-ICR/MS, we can figure out the sulfur-containing unannotated metabolites in our work, at least list the elemental compositions to indicate that the sulfur-containing substances in cerebellum might be those which are affected by genetic manipulation or environmental influence.

### 3.3. Annotation of metabolic changes

The non-targeted method impelled by the highly sensitive instrument in conjunction with multivariate statistics with high-dimensional annotated or un-annotated variables, offers the possibility to integrate the metabolic perturbation in the cerebellum induced by genetic modification or environmental influence. For

the first investigation on AD model, amino acids and amino acid conjugates were putatively identified (all mass errors are less than 0.5 ppm). The levels of the essential amino acids: phenylalanine, tyrosine, leucine/isoleucine, tryptophan and histidine, increased from 4.65-fold to 11.60-fold in Tg samples compared to non-Tg samples. Notably, in respect to methionine sulfoxide (MetO), it is well known that the methionine sulfoxide reductase system is responsible for reducing MetO to methionine, which is able to scavenge oxidants. The enhanced level of MetO may indicate that methionine sulfoxide reductase was inhibited in cerebellum, which is consistent with other report [25]. The up-regulation of amino acid conjugates, such as argininosuccinate, phenylacetylglutamine, was also observed in Tg mice (Table 1). Salicylurate, an acyl glycine, exhibited the unique peak in Tg cerebellar tissues, suggesting that the biosynthesis of salicylurate is associated with cerebellar pathology of AD. Although the concentration of salicylurate was lower than the limit of detection under our experimental conditions in non-Tg samples, it is still covered in all the Tg samples. As a matter of fact, the excretion of certain acyl glycines is increased in several inborn errors of metabolism, suggesting that salicylurate could be considered as the potential biomarker for discrimination of Tg mice and non-Tg littermates [26]. Xanthosine, xanthine and urate in purine metabolism as well as the organic acids were elevated significantly. Surprisingly, however, inosine and guanosine in purine metabolism was detected in reduced level. The metabolic dysregulation in purine metabolism was proposed in Fig. 2. Previously, the lack of inosine was observed in another AD murine model: senescence-prone 8 (SAMP8) [27]. Moreover, guanosine was demonstrated to exert important neuroprotective and neuromodulator roles in the central nervous system [28]. Thus, metabolism disequilibrium in Tg CRND8 mice reveals the attenuation of inosine and guanosine in cerebellum losing the neuroprotective functions and linking to Abeta toxicity in a good agreement with previous reports.

Of particular interest is to identify the ion at *m*/*z* 190.07209, the unique candidate was found in Metlin database and considered to be 2-amino-3,7-dideoxy-D-threo-hept-6-ulosonic acid (ADH). Indeed, ADH synthase could catalyze the biosynthesis of aromatic amino acids in the archaeal pathway [29]. But ADH synthase's function in neurodegenerative disease remains to be explored. Nevertheless, in line with the elevated levels of aromatic amino acids, such as phenylalanine, tyrosine and tryptophan in our results, the up-regulated ADH indicated the increased ADH synthase activity in cerebellum in Tg CRND8 mice compared to non-Tg littermates. Another potential biomarker was observed on the ion at *m*/*z* 161.00914 in negative ion mode. It was putatively identified to be 4-hydroxy-2-oxoglutarate which is a substrate for fructose-bisphosphate aldolase A and involved in the hydroxylation of 2-oxoglutarate or the reversible cleavage of 2-keto-4-hydroxyglutarate, yielding pyruvate plus glyoxylate [30]. Taken together, we can conclude that the metabolic perturbation which involves amino acid biosynthesis and purine metabolism in cerebellum reveals A$\beta$ toxicity widely affecting the brain of Tg mice. It is strikingly that guanosine and inosine may serve the salvage pathways for other purine metabolite biosynthesis, which can be seen in Fig. 2.

In addition to genetic modification, metabolic signature in cerebellum could also be disturbed by environmental toxicant TCDD. In the results of the discriminant masses, several differentiating metabolites were tentatively identified by high accuracy mass analysis in ESI(−) FT-ICR/MS (Table 2). Interestingly, biosynthesis of amino acids was down-regulated by TCDD exposure in comparison to control group, which is opposite to the changes in Tg mice versus non-Tg littermates. Both MetO and methionine were down-regulated in cerebellum caused by TCDD exposure, may due to the decreased amino acid synthesis. Fatty acids as well as fatty acid conjugated metabolites including N-acyl taurine (N-palmitoyl taurine,

**Table 1**
The statistically significant metabolites in Tg mice versus non-Tg littermates.

| Name | Formula | Mass error (ppm) | Fold-change (*P* value) | Metabolite class |
|---|---|---|---|---|
| Phenylalanine | $C_9H_{11}NO_2$ | −0.1 | ↑[b]5.98 (3.23E−03) | Amino acids and amino acid conjugates |
| Tyrosine | $C_9H_{11}NO_3$ | −0.2 | ↑4.65 (4.93E−03) | |
| Tryptophan | $C_{11}H_{12}N_2O_2$ | −0.1 | ↑5.95 (1.15E−03) | |
| Histidine | $C_6H_9N_3O_2$ | −0.0[a] | ↑11.60 (5.24E−05) | |
| Methionine sulfoxide | $C_5H_{11}NO_3S$ | −0.1 | ↑2.80 (3.76E−03) | |
| L-Argininosuccinate | $C_{10}H_{18}N_4O_6$ | 0.2 | ↑25.04 (1.97E−03) | |
| Phenylacetylglutamine | $C_{13}H_{16}N_2O_4$ | 0.3 | ↑18.23 (2.08E−04) | |
| O-Oxalylhomoserine | $C_6H_9NO_6$ | −0.2 | ↑1.66 (1.13E−03) | |
| N-Methyl-L-glutamate/O-Acetyl-L-homoserine | $C_6H_{11}NO_4$ | −0.1 | ↑1.82 (2.65E−04) | |
| Salicylurate | $C_9H_9NO_4$ | 0.1 | ↑Tg[c] (6.95E−03) | |
| Hippurate | $C_9H_9NO_3$ | 0 | ↑25.32 (8.18E−04) | |
| 2-Oxo-3-hydroxy-4-phosphobutanoate | $C_4H_7O_8P$ | 0 | ↑4.83 (1.39E−03) | |
| Inosine | $C_{10}H_{12}N_4O_5$ | 0 | ↓5.49 (5.75E−03) | Purines and purine derivatives |
| Xanthosine | $C_{10}H_{12}N_4O_6$ | 0.1 | ↑Tg (1.59E−05) | |
| Xanthine | $C_5H_4N_4O_2$ | 0 | ↑8.02 (2.85E−04) | |
| Urate | $C_5H_4N_4O_3$ | −0.1 | ↑3.89 (6.20E−04) | |
| Guanosine | $C_{10}H_{13}N_5O_5$ | −0.1 | ↓22.31 (5.95E−03) | |
| 3-Hydroxy-3-methylglutarate | $C_6H_{10}O_5$ | −0.1 | ↑3.30 (2.49E−04) | Organic acids |
| 4-Hydroxy-2-oxoglutarate | $C_5H_6O_6$ | 0 | ↑11.58 (2.01E−05) | |
| Leukotriene A4 | $C_{20}H_{30}O_3$ | 0 | ↑1.92 (4.25E−02) | Fatty acids in arachidonic acid metabolism |
| 5-Hydroxyeicosatetraenoate | $C_{20}H_{32}O_3$ | −0.1 | ↑1.94 (2.65E−02) | |
| Prostaglandin A2 | $C_{20}H_{30}O_4$ | −0.1 | ↑2.56 (1.50E−02) | |
| Prostaglandin B1 | $C_{20}H_{32}O_4$ | 0 | ↑2.30 (1.46E−02) | |
| Prostaglandin H2 | $C_{20}H_{32}O_5$ | 0.1 | ↑2.42 (2.01E−02) | |
| Prostaglandin F2alpha | $C_{20}H_{34}O_5$ | 0 | ↑2.54 (7.77E−03) | |
| Prostaglandin F1alpha | $C_{20}H_{36}O_5$ | 0 | ↑2.19 (2.47E−02) | |
| Prostaglandin G2 | $C_{20}H_{32}O_6$ | −0.3 | ↑2.54 (1.52E−02) | |
| 6-Keto-prostaglandin F1alpha | $C_{20}H_{34}O_6$ | 0 | ↑2.54 (6.06E−03) | |
| 2-Amino-3,7-dideoxy-D-threo-hept-6-ulosonic acid | $C_7H_{13}NO_5$ | 0 | ↑3.16 (1.69E−04) | Other metabolite |

[a] 0.0 denotes the mass error less than 0.05 ppm.
[b] ↑ denotes the metabolite elevated in Tg versus non-Tg mice; ↓ denotes the metabolite decreased in Tg versus non-Tg mice.
[c] Tg denotes the peaks were unique in all the cerebellum samples of Tg mice and cannot detected in non-Tg samples.

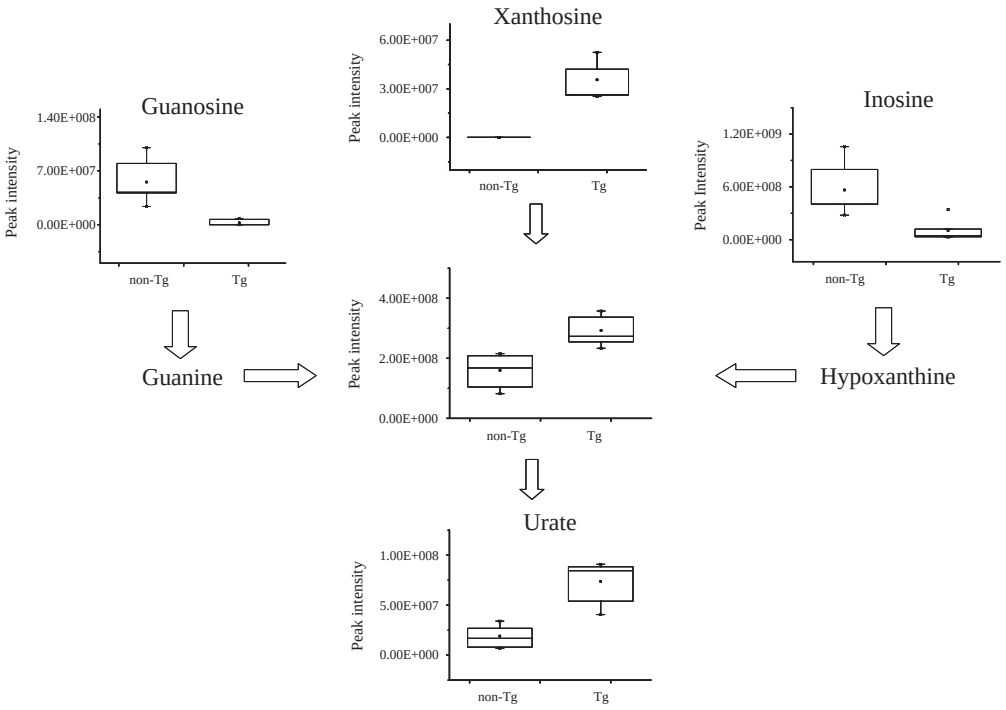


**Fig. 2.** Perturbation of purine metabolism. The decreased levels of guanosine and inosine while the increased levels of xanthosine, xanthine and urate in cerebellum tissues of Tg mice compared to those of non-Tg littermates.

**Table 2**
The statistically significant metabolites in mice exposed to TCDD dosage versus control group.

| Name | Formula | Mass error (ppm) | Fold-change (*P* value) | Metabolite class |
|---|---|---|---|---|
| Phenylalanine | $C_9H_{11}NO_2$ | −0.4 | ↓[b]2.79 (1.97E−03) | Amino acids and amino acid conjugates |
| Methionine | $C_5H_{11}NO_2S$ | −0.3 | ↓1.70(6.25E−03) | |
| Methionine sulfoxide | $C_5H_{11}NO_3S$ | −0.1 | ↓3.15 (3.14E−03) | |
| Glutamylalanine | $C_8H_{14}N_2O_5$ | −0.1 | ↓2.04 (3.97E−03) | |
| N-Acetyl-aspartyl-glutamate | $C_7H_{15}O_{10}P$ | 0.1 | ↓1.70 (2.70E−03) | |
| Cytidine | $C_9H_{13}N_3O_5$ | −0.3 | ↓6.82 (1.58E−03) | Nucleoside analogs |
| Fatty acid C20:3 | $C_{20}H_{34}O_2$ | −0.0[a] | ↑1.38 (3.86E−04) | |
| Fatty acid C18:2 | $C_{18}H_{32}O_2$ | −0.1 | ↑1.31 (5.91E−04) | Fatty acids and fatty acid conjugates |
| Fatty acid C18:3 | $C_{18}H_{30}O_2$ | −0.1 | ↑1.19(1.78E−03) | |
| Fatty acid C22:5 | $C_{22}H_{34}O_2$ | 0.2 | ↑1.30(2.36E−03) | |
| Fatty acid C20:2 | $C_{20}H_{36}O_2$ | 0.1 | ↑1.28(2.62E−03) | |
| Fatty acid C22:6 | $C_{22}H_{32}O_2$ | 0.9 | ↑1.39 (2.63E−03) | |
| Fatty acid C24:6 | $C_{24}H_{36}O_2$ | | ↑1.36 (3.15E−03) | |
| N-palmitoyl taurine | $C_{18}H_{37}NO_4S$ | 0.2 | ↑1.53 (9.71E−05) | |
| N-oleoyl taurine | $C_{20}H_{39}NO_4S$ | 0.4 | ↑1.38 (1.31E−04) | |
| N-linoleoyl taurine | $C_{20}H_{37}NO_4S$ | 0.3 | ↑1.86 (1.31E−04) | |
| N-arachidonoyl taurine | $C_{22}H_{37}NO_4S$ | 0.3 | ↑1.40 (1.22E−03) | |
| N-stearoyl taurine | $C_{20}H_{41}NO_4S$ | 0.4 | ↑1.77 (4.00E−03) | |
| N-palmitoyl GABA | $C_{20}H_{39}NO_3$ | 0.2 | ↑1.78(1.02E−04) | |
| N-docosahexaenoyl GABA | $C_{26}H_{39}NO_3$ | 0.2 | ↑2.46(1.02E−04) | |
| N-stearoyl GABA | $C_{22}H_{43}NO_3$ | −0.1 | ↑1.61 (5.60E−04) | |
| Leukotriene A4 | $C_{20}H_{30}O_3$ | 0.1 | ↓1.81 (6.00E−03) | Fatty acids in arachidonic acid metabolism |
| 5-Hydroxyeicosatetraenoate | $C_{20}H_{32}O_3$ | 0.1 | ↓1.53 (1.90E−02) | |
| Prostaglandin A2 | $C_{20}H_{30}O_4$ | 0.1 | ↓1.80 (1.67E−02) | |
| Prostaglandin B1 | $C_{20}H_{32}O_4$ | 0.2 | ↓1.87 (1.25E−02) | |
| Prostaglandin E3 | $C_{20}H_{30}O_5$ | 0.1 | ↓2.32 (7.38E−03) | |
| Prostaglandin H2 | $C_{20}H_{32}O_5$ | 0.3 | ↓2.64 (7.05E−03) | |
| Prostaglandin F2alpha | $C_{20}H_{34}O_5$ | 0.3 | ↓1.73 (2.51E−02) | |
| Prostaglandin F1alpha | $C_{20}H_{36}O_5$ | 0.3 | ↓1.66 (2.74E−02) | |
| Prostaglandin G2 | $C_{20}H_{32}O_6$ | −0.2 | ↓2.95 (6.80E−03) | |
| 6-Keto-prostaglandin F1alpha | $C_{20}H_{34}O_6$ | 0.3 | ↓2.00 (1.70E−02) | |
| Glucose | $C_6H_{12}O_6$ | −0.3 | ↓1.82(4.19E−05) | Glucose metabolism |
| D-Ribose 5-phosphate | $C_5H_{11}O_8P$ | −0.2 | ↑1.86 (9.41E−04) | |
| D-Sedoheptulose 7-phosphate | $C_7H_{15}O_{10}P$ | 0.2 | ↓1.70(9.63E−04) | |
| Inosine 5′-monophosphate | $C_{10}H_{13}N_4O_8P$ | 0.2 | ↑2.36(1.12E−04) | Purine metabolism |
| Guanosine 5′-monophosphate | $C_{10}H_{14}N_5O_8P$ | 0.4 | ↑2.01(1.33E−05) | |
| Glyceryl phosphate | $C_3H_9O_6P$ | −0.3 | ↑1.44 (2.80E−03) | Energy metabolism |
| Adenosine 5′-monophosphate | $C_{10}H_{14}N_5O_7P$ | 0.2 | ↑1.55 (2.75E−03) | |

[a] 0.0 denotes the mass error less than 0.05 ppm.
[b] ↑ denotes the metabolite elevated in mice exposed to TCDD versus control group; ↓ denotes the metabolite decreased in mice exposed to TCDD versus control group.

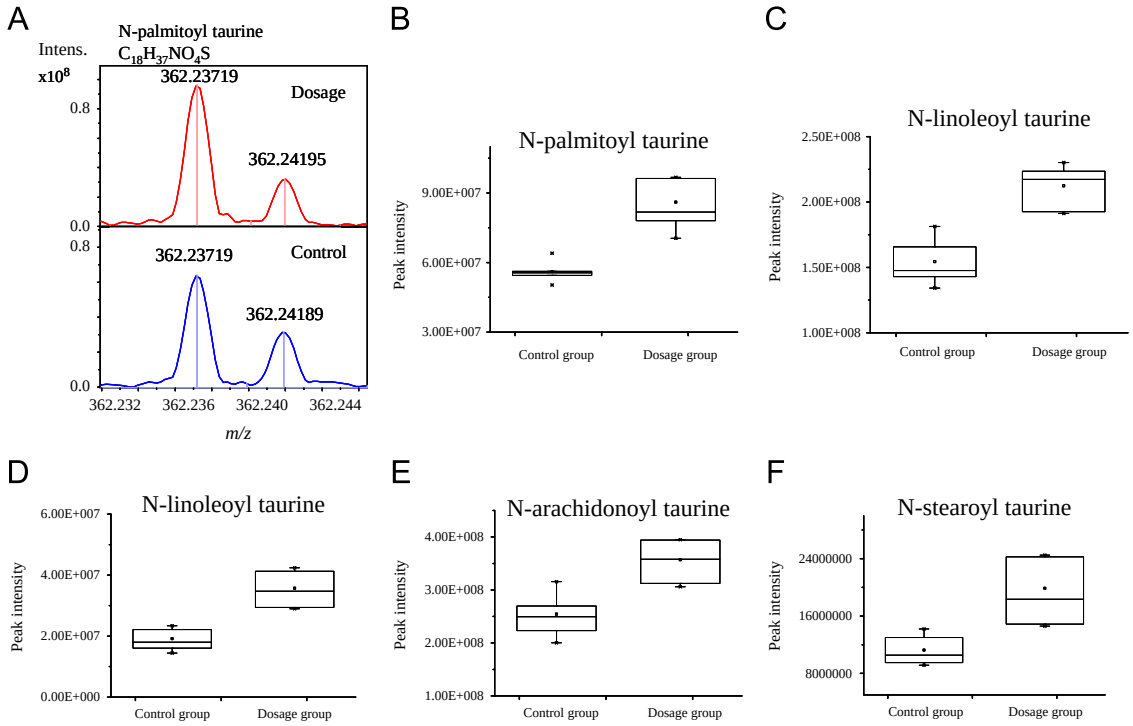


**Fig. 3.** The ion at *m*/*z* 362.23719 was assigned to be $C_{18}H_{37}NO_4S$, corresponding to N-palmitoyl taurine. The elevated level of N-palmitoyl taurine in a dosage sample compared to a control sample was observed, relative to the neighboring ion at *m*/*z* 362.24195 (A). The box plots show the significant changes of N-acyl taurine between TCDD dosage group and control group: N-palmitoyl taurine (B), N-oleoyl taurine (C), N-linoleoyl taurine (D), N-arachidonoyl taurine (E), N-stearoyl taurine (F).

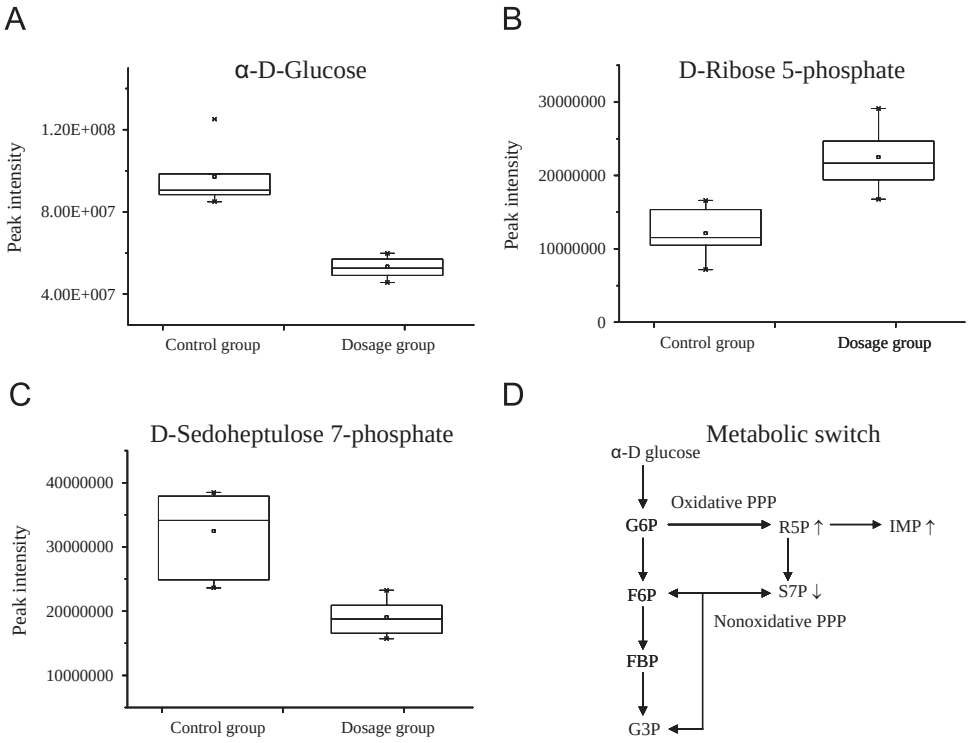


**Fig. 4.** In TCDD study, glucose uptake decreased significantly (A) while the enhanced level of R5P (B) and decreased level of S7P (C) in cerebellum were observed when the mice were exposed to TCDD. The metabolic switch induced TCDD exposure was proposed from nonoxidative arm of PPP to oxidative PPP. G6P: glucose 6-phosphate; F6P: fructose 6-phosphate; FBP: fructose 1,6-bisphosphate; G3P: glyceraldehyde 3-phosphate; R5P: ribose 5-phosphate; S7P: sedoheptulose 7-phosphate; IMP: inosine 5′-monophosphate.

N-oleoyl taurine, N-linoleoyl taurine, N-arachidonoyl taurine and N-stearoyl taurine) and N-acyl gamma-aminobutyric acid (GABA) (N-palmitoyl GABA, N-docosahexaenoyl GABA and N-stearoyl GABA) increased pronouncedly after TCDD exposure (Fig. 3 and Fig. S5). The obtained results suggested that fatty acid or fatty acid conjugate accumulation would be a crucial phenotype in cerebellum. Of particular interest is glucose metabolism. Glucose uptake is suppressed in cerebellum when TCDD exposure occurred (Fig. 4A). Surprisingly,

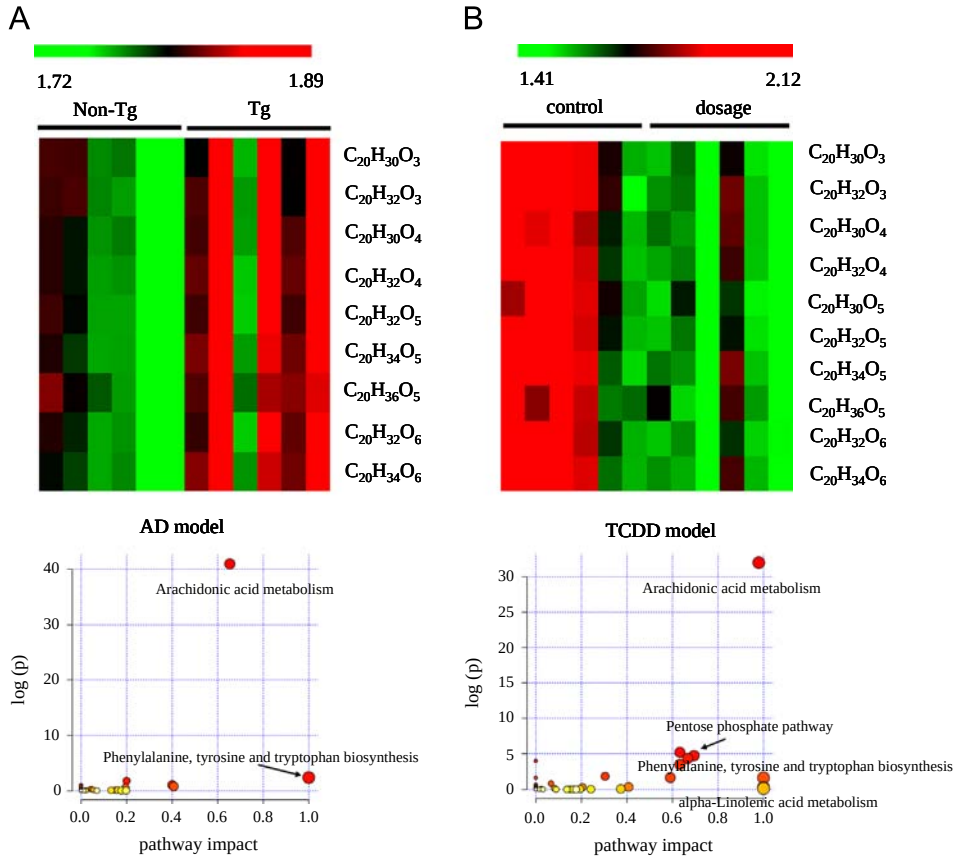


**Fig. 5.** Heat maps of the intermediate metabolites in arachidonic acid metabolism denoted by elemental compositions in AD model (A1) and the pathway analysis for Tg CRND8 of AD model (A2); heat map of the intermediate metabolites in arachidonic acid metabolism denoted by elemental compositions in TCDD model (B1) and the pathway analysis for TCDD exposure mouse model (B2).

D-ribose 5-phosphate was enhanced whereas D-sedoheptulose 7-phosphate decreased markedly (Fig. 4B and C), indicating metabolic channeling to oxidative pentose phosphate pathway (PPP) which is induced by TCDD exposure. Subsequently, the oxidative branch of PPP yields nucleotides as expected. In line with our expectation, inosine 5′-monophosphate and guanosine 5′-monophosphate in purine metabolism were found to be up-regulated, indicating that purine salvage pathway might be necessary for energy demand in cerebellum which is in good agreement with hippocampus.[10] One of the proposed metabolic pathways was visualized in Fig. 5D. The significant changes of glyceryl phosphate and adenosine 5′-monophosphate indicated that energy metabolism in cerebellum was disturbed, too.

To analyze the metabolic pathways, the KEGG IDs with tentative identification of the metabolites were filled into the MetaboloAnalyst database for interpretation. As a result, arachidonic acid metabolism was highlighted in both models (Fig. 5). More interestingly, the fold-changes of eicosanoids in cerebellum tissues are similar to those in hippocampus tissues in the comparison of Tg to non-Tg sample set [31]. Furthermore, the enhanced levels of the intermediate metabolites of arachidonic acid metabolism in Tg mice versus non-Tg littermates as well as the reduced levels of the intermediate metabolites in TCDD dosage group versus control group were visualized in heat maps. This again displays the opposite phenotypes in two murine models affected by genetic modification or environmental toxin.

The ultrahigh resolution mass spectrometry enables highly sensitive measurement and yields very fine mass spectra for discriminating signals of the tested groups, although most of them cannot be identified in biological databases, such as MassTRIX and Metlin. Nevertheless, the possible assignments from highly accurate masses provide the biological annotation to mirror the metabolic changes in cerebellum caused by genetic modification or environmental toxin. At the same time, where scientists claim that the cerebellum issue is less affected toward genetic modification or toxic environmental factors, we show in this work and for the first time that significant changes are taking place in the cerebellum by displaying the highly resolved mass profiles. These new findings could be rendered as preliminary investigations which need further follow ups in the near future.

## 4. Conclusions

Apart from the conventional concept, cerebellum could be affected by genetic and/or environmental alternations. Cerebellum, at least in Tg CRND8 mice as well as the wild type mice exposed to TCDD, could not be resistant to the toxic effects by such genetic factors and/or environmental conditions. Both of them appear to play important roles in the complex etiology of neurotoxicity including the development of AD. Such new and rapid procedure is presented for measurement, relative quantification, and putative identification of metabolites in biological samples. Although we could not unambiguously identify the structure of the metabolites yet, the putatively identified metabolites provided the underlying clues. Nevertheless, biosynthesis of amino acids and amino acid conjugates display the opposite phenotypes in these two mouse models. By combining all the differentiating metabolites, mapping the metabolic traits could delineate the toxic effects of A$\beta$ or TCDD in cerebellar tissues of the two murine models due to gene mutant and environmental toxicant, respectively. This highlights again that metabolic phenotypes are the amplified output to uncover the gene functions and/or the roles of the environment stressors.

## Acknowledgments

Financial supports from General Fund (HKBU200310) from Research Grant Council of Hong Kong SAR, Interdisciplinary Research Fund (IRMC/12–13/1A) from Hong Kong Baptist University and General Research Fund from National Natural Science Foundation of China (21377106) are acknowledged. Dr. Shuhai Lin was supported by German Academic Exchange Service (DAAD) Scholarship (A/12/00412) for the research stay in Germany.

## Appendix A. Supplementary material

Supplementary data associated with this article can be found in the online version at http://dx.doi.org/10.1016/j.talanta.2013.09.019.

## References

[1] J.L. Cummings, H.V. Vinters, G.M. Cole, Z.S. Khachaturian, Neurology 51 (1998) S2-17. (discussion S65-17).
[2] T.L. Spires, B.T. Hyman, NeuroRx 2 (2005) 423–437.
[3] H.J. Kim, S.C. Chae, D.K. Lee, B. Chromy, S.C. Lee, Y.C. Park, W.L. Klein, G. A. Krafft, S.T. Hong, FASEB J. 17 (2003) 118–120.
[4] J. Du, B. Sun, K. Chen, L. Zhang, S. Liu, Q. Gu, L. Fan, N. Zhao, Z. Wang, PLoS One 4 (2009) e5530.
[5] S. Dudal, P. Krzywkowski, J. Paquette, C. Morissette, D. Lacombe, P. Tremblay, F. Gervais, Neurobiol. Aging 25 (2004) 861–871.
[6] M.A. Chishti, D.S. Yang, C. Janus, A.L. Phinney, P. Horne, J. Pearson, R. Strome, N. Zuker, J. Loukides, J. French, S. Turner, G. Lozza, M. Grilli, S. Kunicki, C. Morissette, J. Paquette, F. Gervais, C. Bergeron, P.E. Fraser, G.A. Carlson, P. S. George-Hyslop, D. Westaway, J. Biol. Chem. 276 (2001) 21562–21570.
[7] L.S. Birnbaum, Toxicol. Lett. 82–83 (1995) 743–750.
[8] S. Lin, Z Yang, Y Shen, Z. Cai, Int. J. Mass Spectrom. 301 (2011) 29–36.
[9] S. Lin, Z. Yang, H. Liu, Z. Cai, Mol. Biosyst. 7 (2011) 1956–1965.
[10] S. Lin, Z. Yang, X. Zhang, Z. Bian, Z. Cai, Talanta 85 (2011) 1007–1012.
[11] D. Ohta, S. Kanaya, H. Suzuki, Curr. Opin. Biotechnol. 21 (2010) 35–44.
[12] C. Leon, I. Rodriguez-Meizoso, M. Lucio, V. Garcia-Canas, E. Ibanez, P. Schmitt-Kopplin, A. Cifuentes, J. Chromatogr. A 1216 (2009) 7314–7323.
[13] D. Ohta, D. Shibata, S. Kanaya, Anal. Bioanal. Chem. 389 (2007) 1469–1475.
[14] J. Jansson, B. Willing, M. Lucio, A. Fekete, J. Dicksved, J. Halfvarson, C. Tysk, P. Schmitt-Kopplin, PLoS One 4 (2009) e6386.
[15] M. Lucio, A. Fekete, C. Weigert, B. Wagele, X.J. Zhao, J. Chen, A. Fritsche, H. U. Haring, E.D. Schleicher, G.W. Xu, P. Schmitt-Kopplin, R. Lehmann, PLoS One 5 (2010) e13317.
[16] R.D. Gougeon, M. Lucio, M. Frommberger, D. Peyron, D. Chassagne, H. Alexandre, F. Feuillat, A. Voilley, P. Cayot, I. Gebefugi, N. Hertkorn, P. Schmitt-Kopplin, Proc. Natl. Acad. Sci. USA 106 (2009) 9174–9179.
[17] S. Bijlsma, I. Bobeldijk, E.R. Verheij, R. Ramaker, S. Kochhar, I.A. Macdonald, B. van Ommen, A.K. Smilde, Anal. Chem. 78 (2006) 567–574.
[18] K. Suhre, P. Schmitt-Kopplin, Nucleic Acids Res. 36 (2008) W481–484.
[19] C. Janus, J. Pearson, J. McLaurin, P.M. Mathews, Y. Jiang, S.D. Schmidt, M. A. Chishti, P. Horne, D. Heslin, J. French, H.T. Mount, R.A. Nixon, M. Mercken, C. Bergeron, P.E. Fraser, P. George-Hyslop St, D. Westaway, Nature 408 (2000) 979–982.
[20] T. Kind, O. Fiehn, BMC Bioinf. 8 (2007) 105.
[21] C. Nobata, P.D. Dobson, S.A. Iqbal, P. Mendes, J. Tsujii, D.B. Kell, S. Ananiadou, Metabolomics 7 (2011) 94–101.
[22] E. Bae, I.J. Yeo, B. Jeong, Y. Shin, K.H. Shin, S. Kim, Anal. Chem. 83 (2011) 4193–4199.
[23] V.V. Lobodin, A.G. Marshall, C.S. Hsu, Anal. Chem. 84 (2012) 3410–3416.
[24] Y.S. Jung, S.J. Kim, Y. Kwon do, Y.C. Kim, Amino Acids 42 (2012) 2095–2102.
[25] S.P. Gabbita, M.Y. Aksenov, M.A. Lovell, W.R. Markesbery, J. Neurochem. 73 (1999) 1660–1666.
[26] L. Bonafe, H. Troxler, T. Kuster, C.W. Heizmann, N.A. Chamoles, A.B. Burlina, N. Blau, Mol. Genet. Metab. 69 (2000) 302–311.
[27] N. Jiang, X. Yan, W. Zhou, Q. Zhang, H. Chen, Y. Zhang, X. Zhang, J. Proteome Res. 7 (2008) 3678–3686.
[28] J.A. Saute, L.E. da Silveira, F.A. Soares, L.H. Martini, D.O. Souza, M. Ganzella, Neurobiol. Learn. Mem. 85 (2006) 206–212.
[29] M. Morar, R.H. White, S.E. Ealick, Biochemistry 46 (2007) 10562–10571.
[30] T.J. Riedel, L.C. Johnson, J. Knight, R.R. Hantgan, R.P. Holmes, W.T. Lowther, PLoS One 6 (2011) e26021.
[31] S. Lin, H. Liu, B. Kanawati, L. Liu, J. Dong, M. Li, J. Huang, P. Schmitt-Kopplin, Z. Cai, Anal. Bioanal. Chem. 405 (2013) 5105–5117.